IEEE Open Journal of
Industry Applications

Received 5 March 2023; revised 17 May 2023; accepted 11 July 2023. Date of publication 18 July 2023;
date of current version 21 September 2023. The review of this article was arranged by Associate Editor S. Kaarthik.

Digital Object Identifier 10.1109/OJIA.2023.3296436

A Practical Approach to Determine Limiter Values of Inverter Control to Maximize Renewable Energy Penetration

SOO HYOUNG LEE [1], DONGHEE CHOI [2], AND SEUNG-MOOK BAEK [3] (Member, IEEE)

[1]Division of Electrical, Electronic and Control Engineering, Kongju National University, Cheonan-si 314701, South Korea
[2]Department of Electrical and Control Engineering, Cheongju University, Chengju 28503, South Korea
[3]Division of Electrical, Electronic and Control Engineering, Kongju National University, Cheonan-si 314701, South Korea

CORRESPONDING AUTHOR: DONGHEE CHOI (e-mail: heechoi@cju.ac.kr)

This work was supported in part by the National Research Foundation of Korea (NRF) grant funded by the Korea government (MSIT) under Grant 2022R1A2C2006688 and in part by the Korea Institute of Energy Technology Evaluation and Planning (KETEP) grant funded by the Korean government (MOTIE) under Grant 20223A10100030 (Development of Synchronous Condenser Model and Power System Inertia Operating Technology).

ABSTRACT The increase in renewable-energy-based generations, such as photovoltaic and wind turbines, inevitably leads to an increase in the number and capacity of inverters connected to the power system. This also increases the voltage on the inverter-connected and adjacent buses. By absorbing reactive power appropriately, it can suppress excessive voltage and increase the potential capacity of real power. Currently, most inverters connected to the power grid are set up in a way that does not involve adjusting the voltage at the point of connection. This means that the inverter controller's limiter settings have not significantly impacted the system's stability after a fault. This article examines the impact of reactive power absorption on grid-connected inverters' stability and limiter values' effects on stability. Additionally, to set the limiter values for a convenient inverter controller, the causes of instability are explained in a phasor diagram, and a method for setting the limiter values using this information is explained. The stability impact analysis and limiter value setting are carried out through accurate EMT model-based simulations. The infinite bus with the equivalent impedance is used for the stability analysis and limiter values setting, and the determined values are verified on the real power system. The simulation is conducted using the power system computer-aided design and electromagnetic transient including dc.

INDEX TERMS High renewable penetration, inverter-connected power system, limiter values determination, reactive power absorb control, stability.

I. INTRODUCTION

The recent global attention on the environment, particularly in light of the COVID-19 pandemic, has highlighted the need to limit temperature increases to under 1.5 °C. This means reducing CO_2 emissions to below 45% of 2010 levels by 2030 [1]. In line with this trend, the Korean government has announced its "renewable energy 3020" plan, which aims to increase the country's use of renewable energy sources by up to 20% by 2030 [2]. However, many renewable energy sources, such as solar and wind, fluctuate.

While the shift toward renewable energy is generally a positive development, some technical challenges still need to be addressed. One example is the issue of voltage stability. Even though the current Korean power system is stable, it may not be able to maintain that stability in the future if a large amount of renewable energy sources is connected to the power grid through power converters [3], [4].

The control system of a traditional synchronous generator typically maintains the voltage at the power generation bus. However, this is different for power-controlled inverters. Even though the voltage may rise due to the real power injection of the inverter, the inverter can counteract this by absorbing reactive power. However, this can be difficult for many inverters operating at or near the unit or zero power factor (for renewable generators/energy storage system (ESS) or STATic synchronous COMpensator (STATCOM),

respectively) from the viewpoint of stability, especially after a fault.

There is a research paper to present sequence-based control with current limiting for fault ride-through of the inverter [5]. In that study, the direct axis controls the direct axis component of the grid voltage to follow the reference value, and the quadrature axis controls the quadrature axis component of the grid voltage to be zero. That study focuses on fault ride-through performance, not reactive power control. A study deals nonunit power factor operation of an H-bridge inverter in a low-voltage microgrid [6]. However, the reactive power consumption in this study is smaller than 10% of real power, so the power factor is larger than 99.5. Considering the *R*/*X* ratio is sometimes larger than 1 in a low-voltage distribution system, the reactive power consumption is too small to maintain voltage. Shuai et al. [7] analyze several different control schemes for fault. However, the control schemes they analyzed include measured voltage in the denominator, which is not preferred for commercial ones due to stability issues caused by measurement sensitivity. A modified droop control has been studied to improve stability [8]. Although that study deals with a power factor between 1 and 0, stability with large faults is not considered. A comprehensive ac fault ride-through strategy has been proposed by Cheng et al. [9]. Although that paper deals with the controls with various power factors, the authors decided to change the current reference during fault. However, most commercial inverters require additional detecting devices to apply the proposed reference change during and after a fault. There is also a positive–negative sequence current controller for low voltage ride through (LVRT) improvement of wind-farms-integrated modular multilevel converter-high voltage direct current (MMC-HVdc) network [10]. Although the authors proposed a current limiter in unbalanced faults, stability after fault clearance is out of their concern. A study on flexible power regulation and limitation of voltage source inverter (VSI) under unbalanced grid faults has been conducted by Cheng et al. [11]. That study successfully limits the power during a fault; however, the authors did not care about the stability after the fault. There is a paper about power and current limiting strategy based on droop controllers [12]. In that, the inverter controller includes limiters for references of output current, so the current was effectively limited. However, that study did not deal with a large event, such as an interconnected bus fault. A study compares inverter control modes for voltage stability during contingencies [13]. However, there is no analysis of limiter effects in large-fault conditions. Several small-signal stability analyses were conducted [14], [15], [16], [17], [18]. Although the studies conducted mathematical analyses, they focused on only normal operations, except in extreme situations (caused by large faults, etc.) where control states exceed boundaries for the inverter's normal operation. An impedance-modeling-based stability analysis was conducted for a three-phase three-level neutral point clamped (NPC) inverter [19]. This method either, however, did not consider the limiter effects. The transient stability of droop-controlled inverter networks was analyzed by Smith et al. [20]. Although the description of the analysis is mathematically detailed, the target of the analysis is composed of mathematical assumptions, not a real inverter model. A stability analysis was conducted with dynamic-phasors-based modeling [21]. Although that method showed the mathematical analysis for droop-controlled inverters, the range of analysis is only normal operation, except for a huge-fault condition. Cao et al. [22] conducted the *D*–*Q* impedance-based stability analysis. Although the analysis is mathematically well, they did not consider the huge-fault condition.

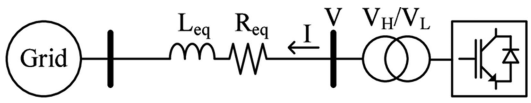

FIGURE 1. Infinite-bus-connected inverter through an impedance.

All these existing papers do not explain how the field engineer stably installs inverters without exact information on existing inverters and power systems. This article proposes a practical approach, which determines limiter values of inverter control, so maximizing renewable energy penetration. The approach involves analyzing the state of the internal proportional–integral controller in phasor representation.

The rest of the article is organized as follows. Section II provides an overview of current inverter control techniques to establish a background and context for the problem being addressed. Then, Section III discusses the controller's internal state variations, particularly identifying the distinctions between normal and fault conditions. Next, the limiter value determination in the equivalent system is given in Section IV. After that, verification using a real power system model is described in Section V. Finally, Section VI concludes this article.

II. CONVENTIONAL INVERTER CONTROL

An infinite-bus-connected inverter through an impedance is shown in Fig. 1.

Real and reactive powers supplied by the inverter can be calculated by

$$P = v_d i_d + v_q i_q \tag{1}$$

$$Q = v_d i_q - v_q i_d \tag{2}$$

where v_d/v_q and i_d/i_q are the direct-/quadrature-axis voltage and current, respectively. In general, the inverter controls real and reactive power independently by making v_q zero using a phase-locked loop (PLL) as:

$$P = V_d I_d \tag{3}$$

$$Q = V_d I_q. \tag{4}$$

To control the power, the inverter uses the bus voltage, V as a reference. Therefore, V_d is determined by the measured voltage because the PLL makes v_q zero. As a result, the real and reactive powers are linearly proportional to I_d and I_q,

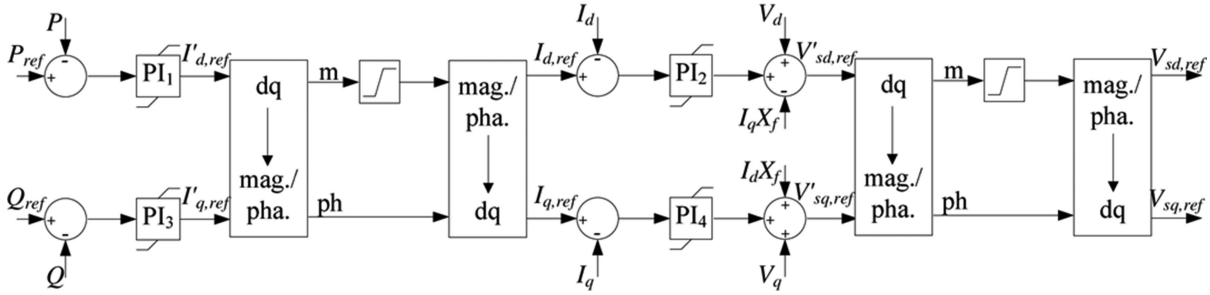

FIGURE 2. Conventional power control block diagram.

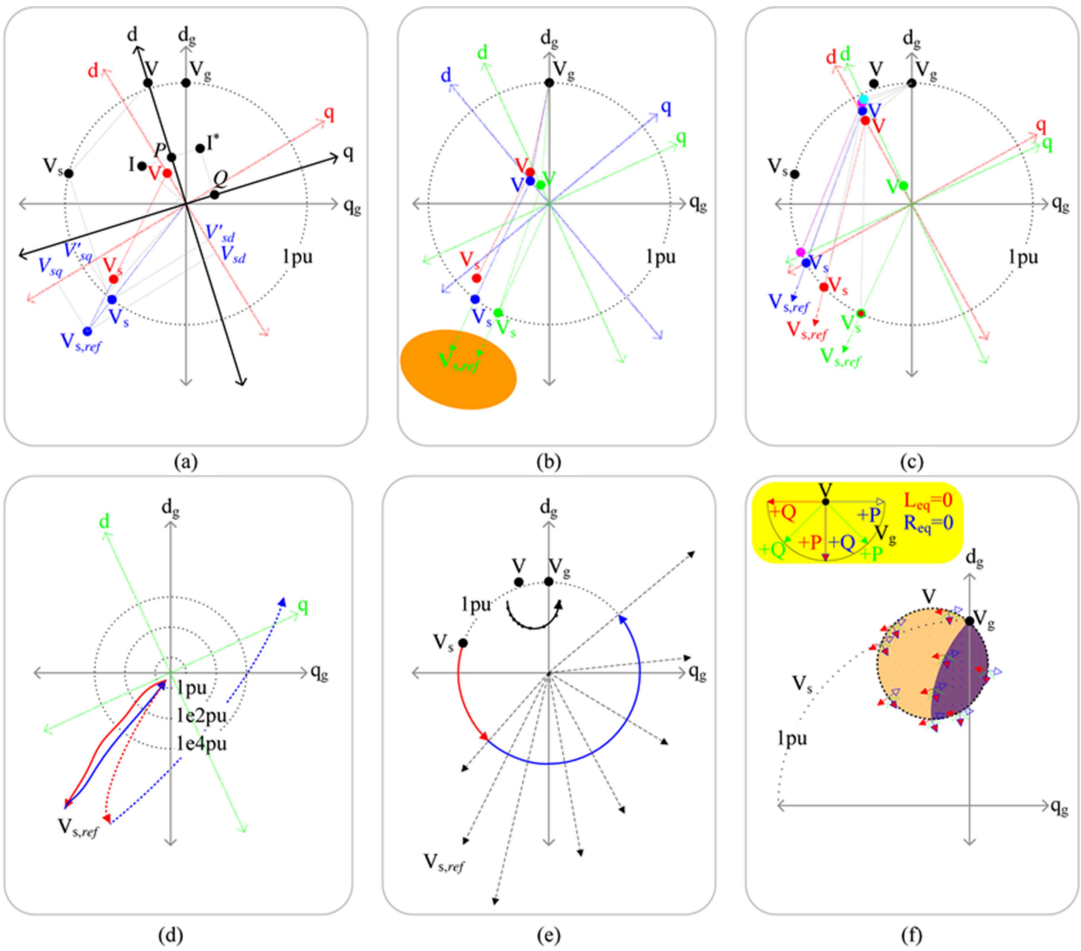

FIGURE 3. Phasor diagrams describing states of inverter operation including (a) grid voltage, POI voltage, and inverter's terminal voltage at prefault and the front part of the fault, (b) terminal voltage reference at fault event, (c) voltages and terminal voltage reference after fault, (d) proper control and malfunction caused by I_{dq} and $I'_{dq,\mathrm{ref}}$ mismatch, (e) voltages by control malfunction, and (f) areas for power supply (orange) and consumption (purple).

respectively. Based on that, conventional power control of the inverter is implemented in Fig. 2. The subscript "ref" means the reference value, and X_f is the impedance of the filter reactor. The maximum value of the inverter's fundamental voltage before the filter per unit system, V_s is $4/\pi$ [23]. The magnitude of V_s is linearly proportional to its reference, $V_{s,\mathrm{ref}}$ (generated by inverse Park's transformation of $V_{sd,\mathrm{ref}}$ and $V_{sq,\mathrm{ref}}$) when it is smaller than 1. It is not linearly proportional when $V_{s,\mathrm{ref}}$ is larger than 1, which is called "overmodulation." For simplification, the maximum value of $V_{s,\mathrm{ref}}$ set 1.

III. INTERNAL STATES OF CONTROLLER

The principle of the inverter operation can be described with the phasors of Fig. 3 as follows.

a) *Prefault and front part of fault*: The direct and quadrature axes referring to grid voltage are denoted as "d_g" and "q_g," respectively. Also, the direct and quadrature axes referring to the point of interconnection (POI) voltage are denoted as "d" and "q." The black points are the initial condition in a steady state before the fault event. In this study, the filter impedance is assumed to be

pure inductance. Therefore, the current lags voltage of "V_s–V" 90°. Assume that the real power reference P_{ref} is positive for convenience of understanding. Also, assume that Q_{ref} is negative due to the control suppressing the voltage increase by the P injection. To consume Q during P injection, I must lead V. Thus, "V_s–V" must lead V more than 90°. At the moment of fault occurrence, the magnitude of V reduces, and the controller tries to increase I by increasing and moving counterclockwise V_s to match P and Q to P_{ref} and Q_{ref} (to the red points). In other words, the voltage magnitude drop reduces P and Q. Then, "P_{ref}–P" and "Q_{ref}–Q" become positive and negative, respectively. Therefore, PI_1 and PI_3 (in Fig. 2) increase $I'_{d,\text{ref}}$ and decrease $I'_{q,\text{ref}}$, respectively. $I'_{dq,\text{ref}}$ is the same with $I_{dq,\text{ref}}$ when the magnitude of I'_{ref} (i.e., vector form of $I'_{dq,\text{ref}}$) is smaller than the current magnitude limiter. PI_2 and PI_4 contribute to the change of V_s making I_{dq} follows $I_{dq,\text{ref}}$, during $V_{s,\text{ref}}$ is inside the circle of 1 p.u. (i.e., $V_s = V_{s,\text{ref}}$). In contrast, V_s cannot make I_{dq} follow $I_{dq,\text{ref}}$ if $V_{s,\text{ref}}$ is outside the circle of 1 p.u. (i.e., $V_s \neq V_{s,\text{ref}}$), so errors might accumulate in the PI controllers (blue points).

b) *Fault duration*: V moves from red to blue point by the change of V_s from red to blue point. Again V_s and V move to green points and remain between the blue and green points while $V_{s,\text{ref}}$ keeps moving in the direction of the orange region. Remark the magnitude of $V_{s,\text{ref}}$ keeps increasing during the fault in accordance with the error accumulation in PI controllers, and becoming larger according to the fault time elapse. Because the PLL follows V, the dq-axis keeps moving between the blue and green axes.

c) *Postfault*: The moment of fault clearance is before the inverter's response. Thus, V_s remains in the red-centered green point (i.e., the last position of fault duration). Then, V moves from green to red based on the power system topology change after fault clearance. Then, the inverter changes V_s to the red point, so V moves to the blue point according to the power system topology. Next, the inverter changes V_s to the blue point, so V moves to the magenta point. After that, the inverter changes V_s to the magenta point, so V moves to the cyan point. Finally, V_s and V converge to the black points, the original states of prefault.

d) $V_{s,\text{ref}}$ *trajectories*: The trajectory of states in (a)–(c) is the result of proper control. In the case of $V_{s,\text{ref}}$ is outside the circle of 1 p.u. (i.e., $V_s \neq V_{s,\text{ref}}$, and V_s is on the circle), I_{dq} cannot follow $I_{dq,\text{ref}}$. The current control errors result in accumulatively increasing $V'_{sd,\text{ref}}$ and decreasing $V'_{sq,\text{ref}}$, so the $V_{s,\text{ref}}$ diverges outside the 1 p.u. circle. There is no guarantee that P(or I_d) and Q(or I_q) errors are released simultaneously. If Q(or I_q) error releases first, the trajectory remains in the third quadrant of the green dq-axis such as solid lines. In contrast, if P(or I_d) error releases first, the trajectory diverges toward the green negative-direct axis (red dotted line). Frequently, $V_{sd,\text{ref}}$ is smaller than −1 p.u. when $V_{sq,\text{ref}}$ becomes between −1 and 1 p.u., and does not come back between −1 and 1 p.u. until $V_{sq,\text{ref}}$ go out of those values (blue dotted line). That is, it never comes back to the circle.

e) *Voltage trajectories*: It is reflected as V_s on the circle of 1 p.u. that $V_{s,\text{ref}}$ trajectory outside the circle. Therefore, the blue dotted line in (d) makes the blue and black solid line trajectories of V_s and V, respectively. The trajectory of V can be a circle if V_s trajectory covers the entire circle of 1 p.u. Although the location of the circle can be changed according to the equivalent impedance, it is useful to predict the trajectory of $V_{s,\text{ref}}$ in (d).

f) *Power direction*: The relative locations of V and V_g determine the sign of P and Q, because it determines the length and direction of I penetration into the grid. The yellow box shows the direction of V_g that results in positive P and Q. For example, the signs are determined based on the blue arrows If the equivalent impedance is pure inductive (i.e., $R_{\text{eq}} = 0$). In other words, I into the grid lags voltage of "V–V_g" 90°, so its direction is the same with V. In the same manner, red arrows show positive P and Q when the equivalent inductance, L_{eq} is zero. The arrows in the dotted circle (i.e., V circle) show the required direction of V_g according to V at several locations. In general, the equivalent impedance includes resistance and inductance; the signs are determined by the green arrows. The relative dq-axis to the $d_g q_g$-axis changes by the location of V, so the directions of the arrows vary as several points of V are shown in the V circle. So roughly, P is positive in the orange region and negative in the purple region (by the green arrows). The large error between negative P and positive P_{ref} makes PI_1 rapidly increase $I'_{d,\text{ref}}$. Therefore, the $V_{s,\text{ref}}$ trajectory shown in (d) moves from the negative to positive along the d-axis. Then, V moves to the orange region where P is positive. If P is sufficiently large to release the accumulated error, $V_{s,\text{ref}}$ moves to the balanced point. If not, $V_{s,\text{ref}}$ keeps moving and enters the purple region again, and the error will be accumulated again and repeated.

The inverter interconnected system is stable if the $V_{s,\text{ref}}$ trajectory is inside the circle of 1 p.u. In contrast, it is unstable if the trajectory is outside the circle. Even inside the circle, however, rotating V_s makes voltage and phase fluctuation, which must be removed as fast as possible. Properly selected limiter values of PI controllers can block the rotation from the start. The limiter values depend on the scale of the event in the grid and the grid topology, so it was difficult to set practically by only investigating individual states of control in a scalar. The proposed methodology investigating the vector state trajectories in the d–q domain helps the user's decision-making to set limiter values.

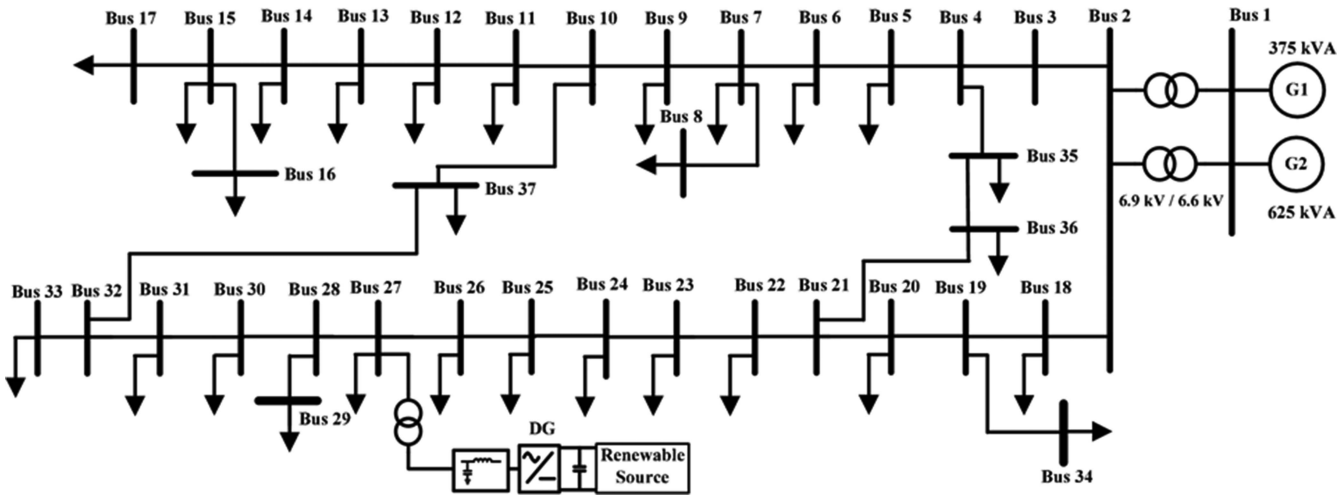

FIGURE 4. Microgrid model based on a real power system on an island in Korea.

TABLE 1. Initial *PI* Control Parameters of the Inverter (see Figs. 5–10)

	PI_1	PI_2	PI_3	PI_4
k_p	1	1	1	1
k_i	10	10	10	10^2
max	10^6	10^6	10^6	10^6
min	-10^6	-10^6	-10^6	-10^6

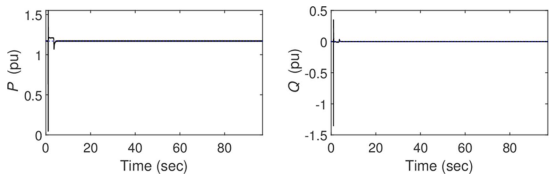

FIGURE 5. Real and reactive powers (black solid-line: P/Q, blue dotted-line: P_{ref}/Q_{ref}) due to a 50-ms fault occurring in 1 s ($Q_{ref} = 0$, Table 1 parameters).

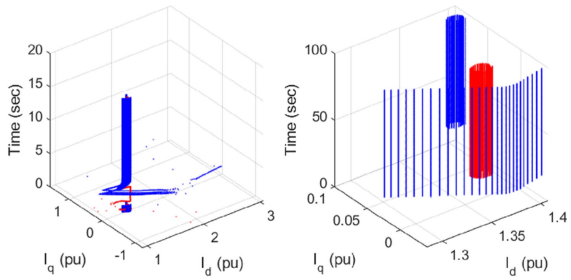

FIGURE 6. $I'_{dq,ref}$ (blue dots) and I_{dq} (red dots) in p.u. due to a 50-ms fault occurring in 1 s; [left] before and [right] after 20 s ($Q_{ref} = 0$, Table 1 parameters).

IV. LIMITER VALUE DETERMINATION IN AN EQUIVALENT SYSTEM

A. REAL AND EQUIVALENT POWER SYSTEM

A microgrid EMT model is implemented as shown in Fig. 4 based on real power system data on an island in Korea. It is assumed that the inverter connection is in bus 27. And then, an equivalent model, such as Fig. 1, is implemented from the viewpoint of the inverter for the limiter value determination. The equivalent electro-motive force (EMF) and impedance are determined as, 6.336 kV and $3.5969 + j3.0295\ \Omega$, respectively. The rated transformer voltages V_H and V_L are set to 6.6 kV and 0.38 kV, respectively. The rated inverter output voltage is set to 0.38 kV. The current magnitude limiter is set to the same as the rated current (i.e., 1.5 p.u.), and the initial limiters of PI_1 and PI_3 are set sufficiently large to ignore their effect.

B. CASE 1 ($Q_{REF} = 0$, 3ϕ-TO-G FAULT OF 2.653 μH)

The initial *PI* control parameters are selected, as shown in Table 1. The initial limiter values are set sufficiently to make space for the *PI* controller's states without reaching the limiter. Initially, P_{ref} and Q_{ref} are set to 1.17 p.u. and 0 p.u. respectively. The POI voltage is 1.05 p.u. in this condition, and the voltage increases according to the real power increase. Therefore, P_{ref} is the maximum power that can be transmitted to the power system by abiding by the grid code. A three-phase-to-ground fault of 2.653 μH (i.e., inductive 1 mΩ) is applied to set up an extreme fault event.

The inverter successfully follows its power references after the fault clearance, as shown in Fig. 5. $I'_{dq,ref}$ is not going far from I_{dq} during the fault event (as shown in the left plots of Fig. 6), so it can return close to I_{dq} fast (i.e., $I_{dq,ref}$ return fast). Due to the magnitudes of $I'_{dq,ref}$ being smaller than 1.5 p.u. (by the current magnitude limiter), they are the same as $I_{dq,ref}$ as shown on the right plots of Fig. 6. The group of blue dots shows $I_{dq,ref}$ movement and the red dots group shows the I_{dq} movement. The differences between $I_{dq,ref}$ and I_{dq} during fault make the PI_2/PI_4 outputs diverge toward a single direction, as shown in the left-hand side of Fig. 7. As a result, $|V_{s,ref}|$ increases much larger than the maximum value of V_s. However, the increased $|V_{s,ref}|$ returns to the controllable region (i.e., inside the green circle) before the returning trajectory

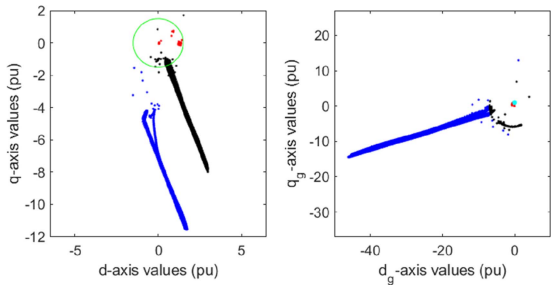

FIGURE 7. [Left] *dq*-axis trajectories of PI_2/PI_4 outputs (blue), V_{dq} (red), and $V'_{sdq,\text{ref}}$ (black) in p.u. with V_{sdq} boundary (green). [Right] $d_g q_g$-axis trajectories of $V'_{s,\text{ref}}$ (blue), V (red), V_s (black), and V_g (cyan) in p.u. ($Q_{\text{ref}} = 0$, Table 1 parameters).

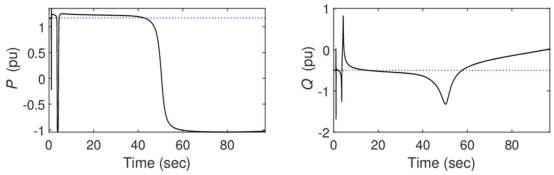

FIGURE 8. Real and reactive powers (black solid-line: *P*/*Q*, blue dotted-line: $P_{\text{ref}}/Q_{\text{ref}}$) due to a 50-ms fault occurring in 1 s ($Q_{\text{ref}} = -0.5$ p.u., Table 1 parameters).

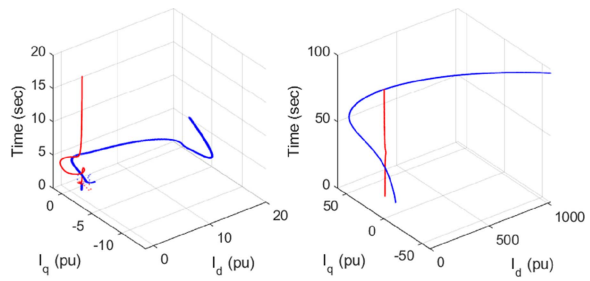

FIGURE 9. $I_{dq,\text{ref}}$ (blue dots) and I_{dq} (red dots) in p.u. due to a 50-ms fault occurring in 1 s; [left] before and [right] after 20 s ($Q_{\text{ref}} = -0.5$ p.u., Table 1 parameters).

differs from the going trajectory (i.e., key performance for returning to normal state). Due to that reason, the conventional power control in the unity power factor operates well without carefully considering limiter values.

C. CASE 2 ($Q_{REF} = -0.5$ P.U., 3ϕ-TO-G FAULT OF 2.653 μH)

As previously mentioned, reactive power absorption is required to increase power acceptance to the power system when the inverter occupies a large portion of the power system. All parameters are set the same as Case 1 except that Q_{ref} is -0.5 p.u. As shown in Fig. 8, the real and reactive power looks approaching their references before about 20 s. The inverter, however, abruptly loses its control after about 40 s. The malfunction is caused by the error accumulation between $I'_{dq,\text{ref}}$ and I_{dq}, as shown in Fig. 9. The error increases after the fault event, even if P and Q approach their references, as shown in Figs. 8 and 9. In other words, the inverter is not properly controlled, even if it seems to control P and Q correctly at a glance. $|I'_{dq,\text{ref}}|$ increases with time, as shown in Fig. 9. Consequently, $I_{dq,\text{ref}}$ is determined by the current magnitude

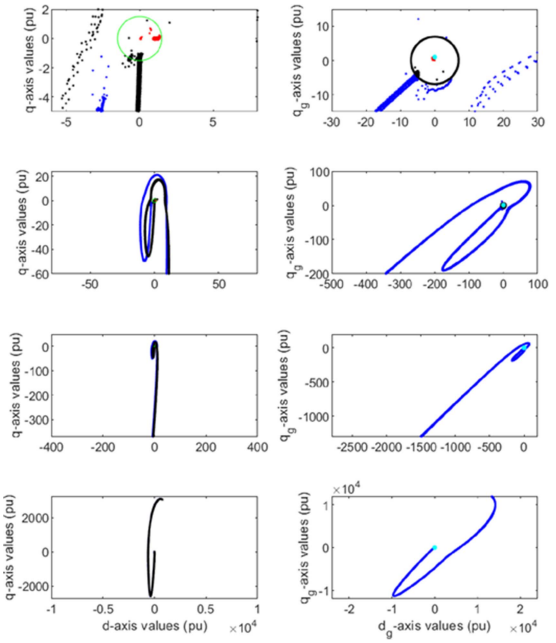

FIGURE 10. [Left] *dq*-axis trajectories of PI_2/PI_4 outputs (blue), V_{dq} (red), and $V'_{sdq,\text{ref}}$ (black) in p.u. with V_{sdq} boundary (green). [Right] $d_g q_g$-axis trajectories of $V'_{s,\text{ref}}$ (blue), V (red), V_s (black), and V_g (cyan) in p.u. ($Q_{\text{ref}} = -0.5$ p.u., Table 1 parameters).

TABLE 2. *PI* Control Parameters of the Inverter (see Figs. 11–13)

	PI_1	PI_2	PI_3	PI_4
k_p	1	1	1	1
k_i	10	10	10	10^2
max	**1.5**	10^6	**1**	10^6
min	**-1.5**	-10^6	**-2**	-10^6

The bold-faced values emphasize the changed values from the previous table.

limiter regardless of the correct control of I_{dq}. As a result, PI_2/PI_4 output increases with time, as shown in the left plots in Fig. 10. It makes $V_{s,\text{ref}}$ go outside the controllable range (black circle) of V_s, as shown on the right plots in Fig. 10. In contrast to Case 1, increased $V_{s,\text{ref}}$ does not return to the controllable region by making the returning trajectory differ from the going trajectory. Due to that reason, the conventional power control cannot operate correctly with reactive power consumption.

The red curve at the left in Fig. 9 is shown as a circle of the following eqaution at the top-to-bottom viewpoint along the time axis:

$$I_d^2 + (I_q + 0.5)^2 = 1.5^2. \tag{5}$$

Therefore, the upper/lower limiters for PI_1 and PI_3 are set as 1.5/$-$1.5 and 1/$-$2, respectively, to minimize errors between the red and blue lines without an impact on the nonfault current (see Table 2).

The real and reactive powers are controlled correctly, as shown in Fig. 11. This is because $I'_{dq,\text{ref}}$ remains near $I_{dq,\text{ref}}$. $I'_{dq,\text{ref}}$ can return to normal control fast after the fault clearance, as shown in Fig. 12. Also, PI_2/PI_4 make $V'_{sdq,\text{ref}}$ remain

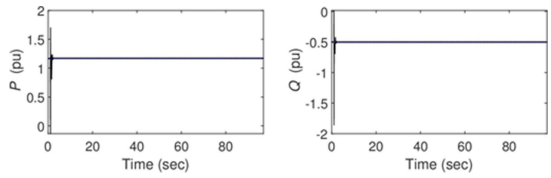

FIGURE 11. Real and reactive powers (black solid-line: P/Q, blue dotted-line: $P_{\text{ref}}/Q_{\text{ref}}$) due to a 50-ms fault occurring in 1 s ($Q_{\text{ref}} = -0.5$ p.u., Table 2 parameters).

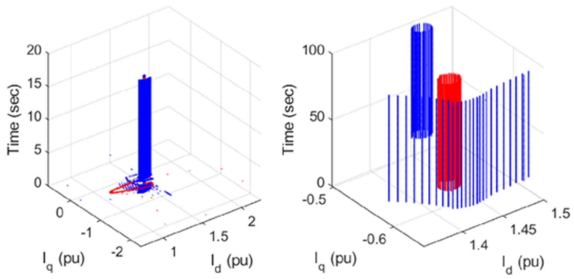

FIGURE 12. $I_{dq,\text{ref}}$ (blue dots) and I_{dq} (red dots) in p.u. due to a 50-ms fault occurring in 1 s; [left] before and [right] after 20 s ($Q_{\text{ref}} = -0.5$ p.u., Table 2 parameters).

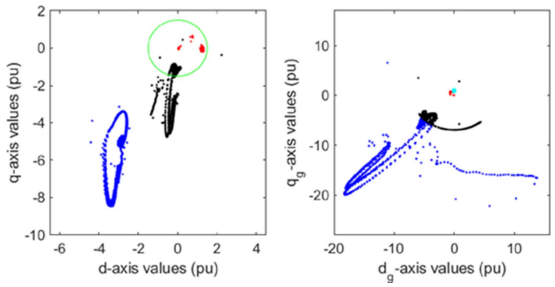

FIGURE 13. [Left] dq-axis trajectories of PI_2/PI_4 outputs (blue), V_{dq} (red), and $V'_{sdq,\text{ref}}$ (black) in p.u. with V_{sdq} boundary (green). [Right] $d_g q_g$-axis trajectories of $V'_{s,\text{ref}}$ (blue), V (red), V_s (black), and V_g (cyan) in p.u. ($Q_{\text{ref}} = -0.5$ p.u., Table 2 parameters).

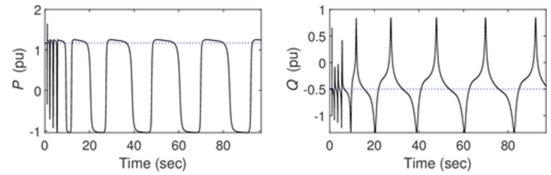

FIGURE 14. Real and reactive powers (black solid-line: P/Q, blue dotted-line: $P_{\text{ref}}/Q_{\text{ref}}$) due to a 50-ms fault occurring in 1 s ($Q_{\text{ref}} = -0.5$ p.u., Table 2 parameters).

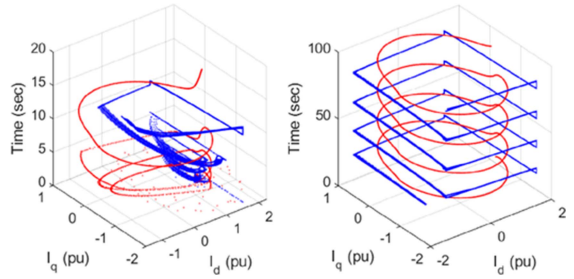

FIGURE 15. $I_{dq,\text{ref}}$ (blue dots) and I_{dq} (red dots) in p.u. due to a 50-ms fault occurring in 1 s; [left] before and [right] after 20 s ($Q_{\text{ref}} = -0.5$ p.u., Table 2 parameters).

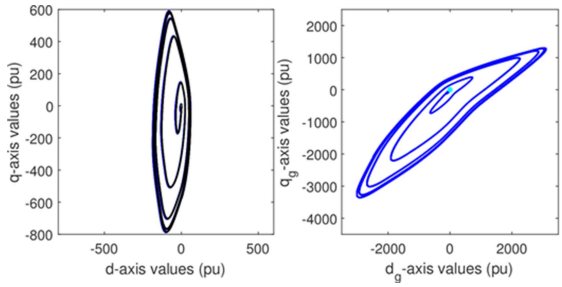

FIGURE 16. [Left] dq-axis trajectories of PI_2/PI_4 outputs (blue), V_{dq} (red), and $V'_{sdq,\text{ref}}$ (black) in p.u. with V_{sdq} boundary (green). [Right] $d_g q_g$-axis trajectories of $V'_{s,\text{ref}}$ (blue), V (red), V_s (black), and V_g (cyan) in p.u. ($Q_{\text{ref}} = -0.5$ p.u., Table 2 parameters).

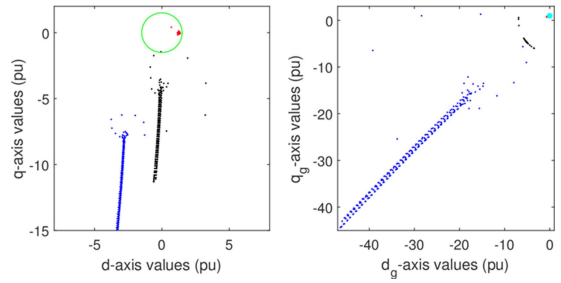

FIGURE 17. Part of Fig. 16: for 0.25 s after fault clearance. [Left] dq-axis trajectories of PI_2/PI_4 outputs (blue), V_{dq} (red), and $V'_{sdq,\text{ref}}$ (black) in p.u. with V_{sdq} boundary (green). [Right] $d_g q_g$-axis trajectories of $V'_{s,\text{ref}}$ (blue), V (red), V_s (black), and V_g (cyan) in p.u. ($Q_{\text{ref}} = -0.5$ p.u., Table 2 parameters).

TABLE 3. *PI* Control Parameters of the Inverter (see Figs. 17–19)

	PI_1	PI_2	PI_3	PI_4
k_p	1	1	1	1
k_i	10	10	10	10^2
max	**1.5**	10^6	**1**	10^6
min	**-1.5**	**-5**	**-2**	**-5**

The bold-faced values emphasize the changed values from the previous table.

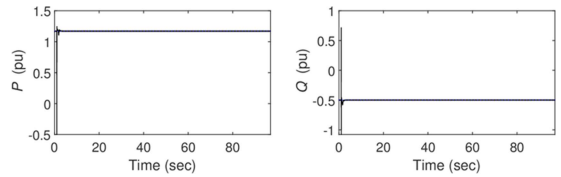

FIGURE 18. Real and reactive powers (black solid-line: P/Q, blue dotted-line: $P_{\text{ref}}/Q_{\text{ref}}$) due to a 50-ms fault occurring in 1 s ($Q_{\text{ref}} = -0.5$ p.u., Table 3 parameters).

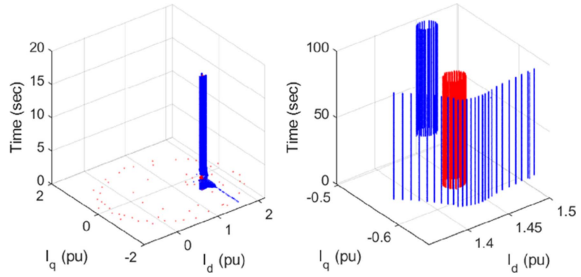

FIGURE 19. $I_{dq,\text{ref}}$ (blue dots) and I_{dq} (red dots) in p.u. due to a 50-ms fault occurring in 1 s; [left] before and [right] after 20 s ($Q_{\text{ref}} = -0.5$ p.u., Table 3 parameters).

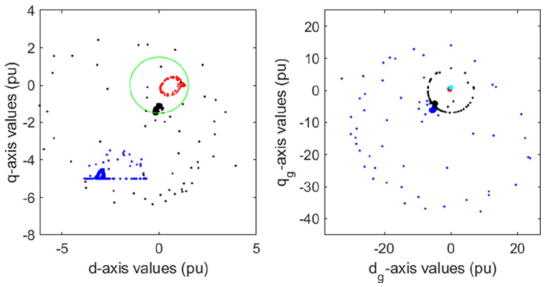

FIGURE 20. [Left] *dq*-axis trajectories of PI_2/PI_4 outputs (blue), V_{dq} (red), and $V'_{sdq,\text{ref}}$ (black) in p.u. with V_{sdq} boundary (green); [right] d_gq_g-axis trajectories of $V'_{s,\text{ref}}$ (blue), V (red), V_s (black), and V_g (cyan) in p.u. ($Q_{\text{ref}} = -0.5$ p.u., Table 3 parameters).

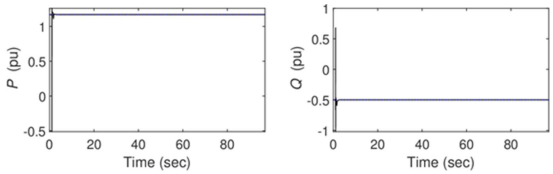

FIGURE 21. Real and reactive powers in real power system (black solid-line: *P/Q*, blue dotted-line: $P_{\text{ref}}/Q_{\text{ref}}$) due to a 50-ms fault occurring in 1 s ($Q_{\text{ref}} = -0.5$ p.u., Table 3 parameters).

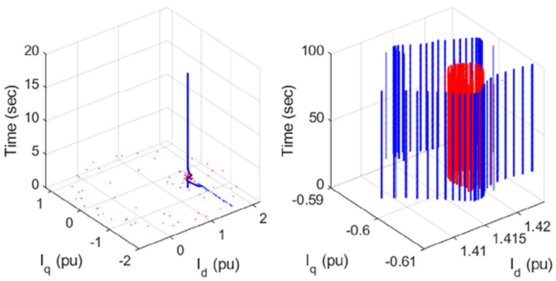

FIGURE 22. $I_{dq,\text{ref}}$ (blue dots) and I_{dq} (red dots) in p.u. in real power system, due to a 50-ms fault occurring in 1 s; [left] before and [right] after 20 s ($Q_{\text{ref}} = -0.5$ p.u., Table 3 parameters).

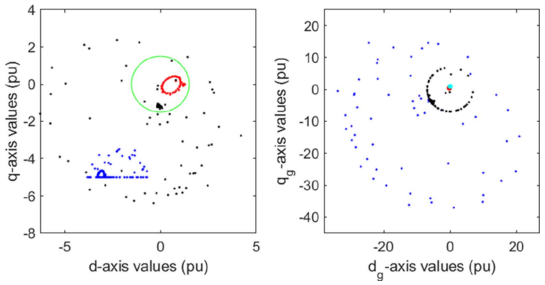

FIGURE 23. [Left] *dq*-axis trajectories of PI_2/PI_4 outputs (blue), V_{dq} (red), and $V'_{sdq,\text{ref}}$ (black) in p.u. with V_{sdq} boundary (green) in real power system; [right] d_gq_g-axis trajectories of $V'_{s,\text{ref}}$ (blue), V (red), V_s (black), and V_g (cyan) in p.u.. ($Q_{\text{ref}} = -0.5$ p.u., Table 3 parameters).

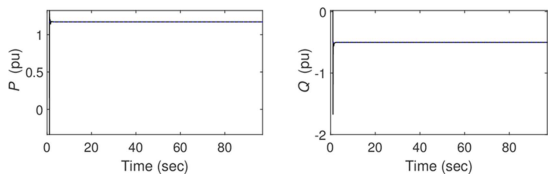

FIGURE 24. Real and reactive powers in real power system (black solid-line: *P/Q*, blue dotted-line: $P_{\text{ref}}/Q_{\text{ref}}$) due to a 50-ms fault occurring in 1 s ($Q_{\text{ref}} = -0.5$ p.u., Table 3 parameters).

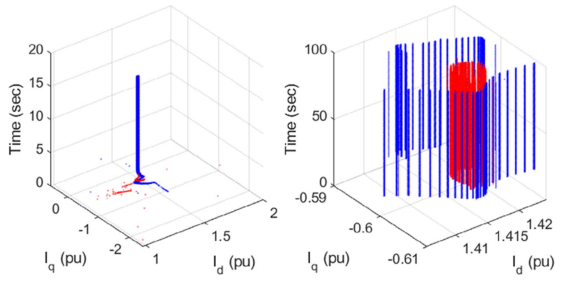

FIGURE 25. $I_{dq,\text{ref}}$ (blue dots) and I_{dq} (red dots) in p.u. in real power system, due to a 50-ms fault occurring in 1 s; [left] before and [right] after 20 s ($Q_{\text{ref}} = -0.5$ p.u., Table 3 parameters).

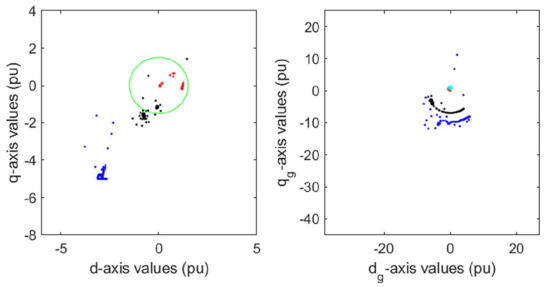

FIGURE 26. [Left] *dq*-axis trajectories of PI_2/PI_4 outputs (blue), V_{dq} (red), and $V'_{sdq,\text{ref}}$ (black) in p.u. with V_{sdq} boundary (green) in real power system; [right] d_gq_g-axis trajectories of $V'_{s,\text{ref}}$ (blue), V (red), V_s (black), and V_g (cyan) in p.u. ($Q_{\text{ref}} = -0.5$ p.u., Table 3 parameters).

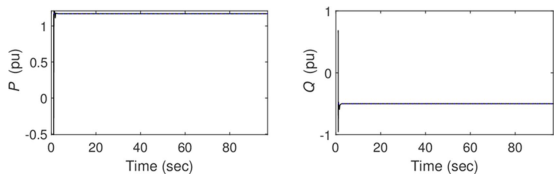

FIGURE 27. Real and reactive powers in real power system (black solid-line: *P/Q*, blue dotted-line: $P_{\text{ref}}/Q_{\text{ref}}$) due to a 50-ms fault occurring in 1 s ($Q_{\text{ref}} = -0.5$ p.u., Table 3 parameters).

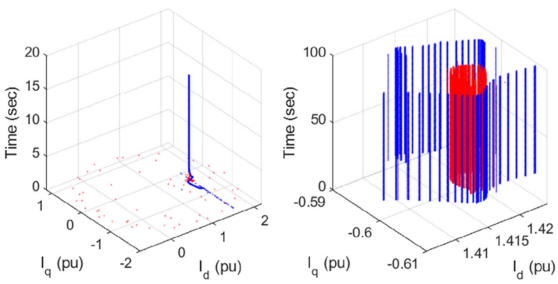

FIGURE 28. $I_{dq,\text{ref}}$ (blue dots) and I_{dq} (red dots) in p.u. in real power system, due to a 50-ms fault occurring in 1 s; [left] before and [right] after 20 s ($Q_{\text{ref}} = -0.5$ p.u., Table 3 parameters).

near V_s boundary due to the minimized error between $I_{dq,\text{ref}}$ and I_{dq}, as shown in the left plots of Fig. 13. In other words, from the viewpoint of the d_gq_g-axis, $V'_{s,ref}$ remains near V_s, as shown in the right plots in Fig. 13. Consequently, $V'_{s,\text{ref}}$ can return inside the V_s boundary after the fault clearance.

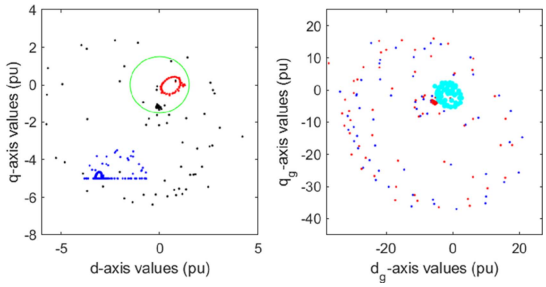

FIGURE 29. [Left] dq-axis trajectories of PI_2/PI_4 outputs (blue), V_{dq} (red), and $V'_{sdq,\text{ref}}$ (black) in p.u. with V_{sdq} boundary (green) in real power system; [right] $d_g q_g$-axis trajectories of $V'_{s,\text{ref}}$ (blue), V (red), V_s (black), and V_g (cyan) in p.u. ($Q_{\text{ref}} = -0.5$ p.u., Table 3 parameters).

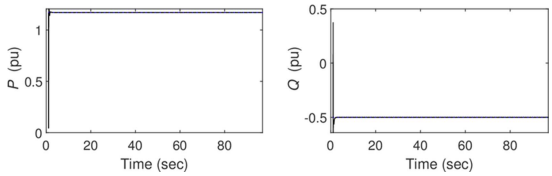

FIGURE 30. Real and reactive powers in real power system (black solid-line: P/Q, blue dotted-line: $P_{\text{ref}}/Q_{\text{ref}}$) due to a 50-ms fault occurring in 1 s ($Q_{\text{ref}} = -0.5$ p.u., Table 3 parameters).

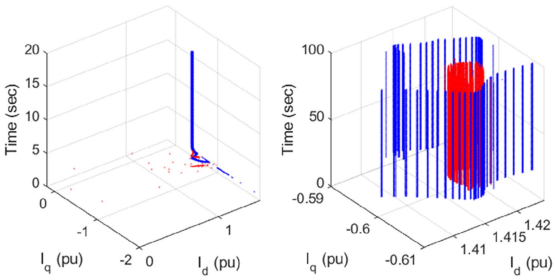

FIGURE 31. $I_{dq,\text{ref}}$ (blue dots) and I_{dq} (red dots) in p.u. in real power system, due to a 50-ms fault occurring in 1 s; [left] before and [right] after 20 s ($Q_{\text{ref}} = -0.5$ p.u., Table 3 parameters).

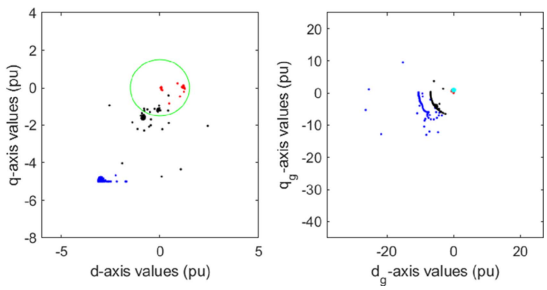

FIGURE 32. [Left] dq-axis trajectories of PI_2/PI_4 outputs (blue), V_{dq} (red), and $V'_{sdq,\text{ref}}$ (black) in p.u. with V_{sdq} boundary (green) in real power system; [right] $d_g q_g$-axis trajectories of $V'_{s,\text{ref}}$ (blue), V (red), V_s (black), and V_g (cyan) in p.u. ($Q_{\text{ref}} = -0.5$ p.u., Table 3 parameters).

D. CASE 3 ($Q_{REF} = -0.5$ P.U., 1ϕ-TO-G FAULT OF 2.653 μH)

A three-phase-to-ground fault is generally considered more severe than a single-phase-to-ground fault in a power system. From the viewpoint of the inverter, however, POI voltage unbalances, caused by the single-phase-to-ground fault, can be a more severe condition for the power control. As shown

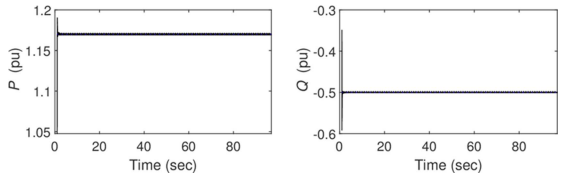

FIGURE 33. Real and reactive powers in real power system (black solid-line: P/Q, blue dotted-line: $P_{\text{ref}}/Q_{\text{ref}}$) due to a 50-ms fault occurring in 1 s ($Q_{\text{ref}} = -0.5$ p.u., Table 3 parameters).

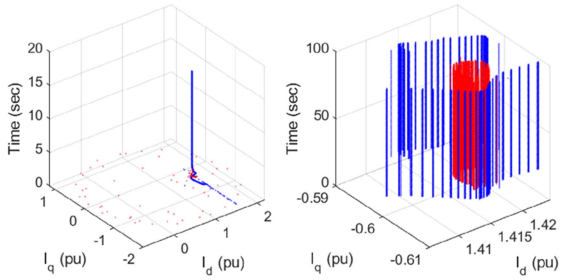

FIGURE 34. $I_{dq,\text{ref}}$ (blue dots) and I_{dq} (red dots) in p.u. in real power system, due to a 50-ms fault occurring in 1 s; [left] before and [right] after 20 s ($Q_{\text{ref}} = -0.5$ p.u., Table 3 parameters).

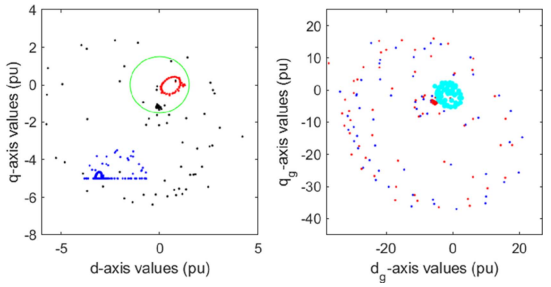

FIGURE 35. [Left] dq-axis trajectories of PI_2/PI_4 outputs (blue), V_{dq} (red), and $V'_{sdq,\text{ref}}$ (black) in p.u. with V_{sdq} boundary (green) in real power system; [right] $d_g q_g$-axis trajectories of $V'_{s,\text{ref}}$ (blue), V (red), V_s (black), and V_g (cyan) in p.u. ($Q_{\text{ref}} = -0.5$ p.u., Table 3 parameters).

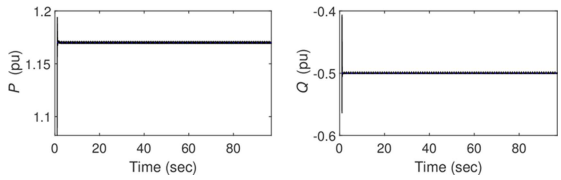

FIGURE 36. Real and reactive powers in real power system (black solid-line: P/Q, blue dotted-line: $P_{\text{ref}}/Q_{\text{ref}}$) due to a 50-ms fault occurring in 1 s ($Q_{\text{ref}} = -0.5$ p.u., Table 3 parameters).

in Fig. 14, the inverter fails to control P and Q even if it was successful in Case 2. This is because the difference between $I_{dq,\text{ref}}$ and I_{dq} is repeated and its magnitude is not reduced with time, as shown in Fig. 15. The repetitive error makes PI_2/PI_4 output also repeat. Therefore, $V'_{sdq,\text{ref}}$ ($V'_{s,\text{ref}}$ in the $d_g q_g$-axis) also repeats, as shown in Fig. 16.

The trajectory of $V'_{sdq,\text{ref}}$ is most outside V_{sdq} boundary even if it does not diverge. This results in the repetitive P and Q in Fig. 14. To stabilize P and Q, the trajectory of $V'_{sdq,\text{ref}}$ needs to return fast to inside V_{sdq} boundary by being near the

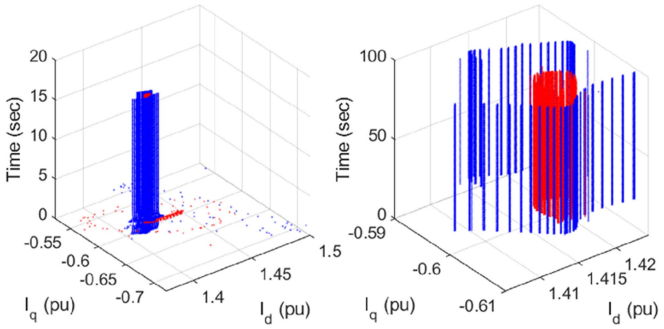

FIGURE 37. $I_{dq,\text{ref}}$ (blue dots) and I_{dq} (red dots) in p.u. in real power system, due to a 50-ms fault occurring in 1 s; [left] before and [right] after 20 s ($Q_{\text{ref}} = -0.5$ p.u., Table 3 parameters).

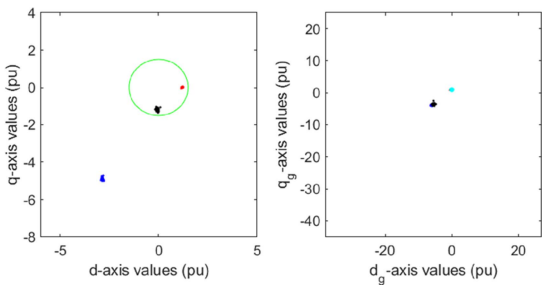

FIGURE 38. [Left] dq-axis trajectories of PI_2/PI_4 outputs (blue), V_{dq} (red), and $V'_{sdq,\text{ref}}$ (black) in p.u. with V_{sdq} boundary (green) in real power system; [right] $d_g q_g$-axis trajectories of $V'_{s,\text{ref}}$ (blue), V (red), V_s (black), and V_g (cyan) in p.u. ($Q_{\text{ref}} = -0.5$ p.u., Table 3 parameters).

boundary. The boundary can be seen by enlarging Fig. 16. After fault clearance, PI_2/PI_4 output goes south due to positive "P_{ref}–P" and negative "Q_{ref}–Q" as described in Fig. 3(d). Therefore, the repetitive trajectory shown in Fig. 16 can be blocked by setting the limiter values to its start point. In this study, the lower limiter for PI_2/PI_4 is set to -5, as shown in Table 3. Then, $V'_{sdq,\text{ref}}$ can remain inside the V_{sdq} boundary. As a result, the inverter successfully controls P and Q, as shown in Fig. 18. I_{dq} successfully flows $I'_{dq,\text{ref}}$ (i.e., $I'_{dq,\text{ref}} = I_{dq,\text{ref}}$), as shown in Fig. 19. All states remain steady (groups of points) except during fault (scattered points), as shown in Fig. 20.

V. VERIFICATION USING REAL POWER SYSTEM MODEL

A. CASE 4 ($Q_{REF} = -0.5$ P.U., 1ϕ-TO-G FAULT OF 2.653 μH)

The inverter is connected to the real microgrid model in Fig. 4 with the determined limiter values. The powers are properly controlled even after fault, as shown in Fig. 21. Also, the current properly follows the reference, as shown in Fig. 22. All states remain steady soon after fault clearance as did in the equivalent circuit, as shown in Fig. 23.

B. CASE 5 ($Q_{REF} = -0.5$ P.U., 3ϕ-TO-G FAULT OF 2.653 μH)

The three-phase to ground fault is less harmful than the single-phase to ground fault, according to Cases 2 and 3. Consequently, the powers are properly controlled, as shown in Fig. 24, and all states remain steady soon after fault clearance, as shown in Fig. 25. The less scatteredness of voltages in Fig. 26 than those in Fig. 23 shows that the three-phase to ground fault is less harmful than the single-phase to ground fault to the inverter control.

C. SUPPLEMENTARY CASES

For Case 6 (Figs. 27– 29), -0.5 p.u. of Q_{ref} and 1ϕ-to-g resistive fault of 1 mΩ is applied. It shows similar results to the inductive fault of Case 4. Thus, the selected parameters are still valid. For Case 7 (Figs. 30– 32), -0.5 p.u. of Q_{ref} and 3ϕ-to-g resistive fault of 1 mΩ is applied. It shows similar results to the inductive fault of Case 5. Thus, the selected parameters are still valid. For Case 8 (Figs. 33– 35), -0.5 p.u. of Q_{ref} and 1ϕ-to-g inductive fault of 265.3 μH is applied. As Section V-B describes, the three-phase-to-ground fault is less harmful than the single-phase-to-ground fault to the inverter control. Thus, only the single-phase-to-ground fault is considered in the following sections. The scatteredness of the voltages in Fig. 35 is much smaller than in the previous cases due to the large fault impedance (i.e., small fault). For Case 9 (Figs. 36– 38), -0.5 p.u. of Q_{ref} and 1ϕ-to-g resistive fault of 100 mΩ is applied. The scatteredness of the voltages in Fig. 38 is similar to that in Fig. 35, regardless of the power factor of the fault. That is, the limiter setting must consider the harshest conditions to cover all less severe cases.

VI. CONCLUSION

This article proposes a practical method to stabilize the inverter control using EMT simulation. It shows the process of stabilizing inverter control by determining limiter values without generating a complicated transfer function. This method helps the field engineer to tune up the limiters. The field engineer can avoid numerous time-based simulations to determine the control parameters for grid stability. Also, it helps to overcome the very complicated analyses based on control theory, which is sometimes practically impossible in a complex real power system.

Designing and tuning all the controllers might be best in case of the entire grid is implemented as a single project. In practice, however, the inverters are installed in the grid independently under their needs. Therefore, the field engineer generally lacks information about the existing inverters. The proposed method does not focus on fine-tuning the inverter, which needs exact information, but focuses on improving stability even if without accurate information.

REFERENCES

[1] V. Masson-Delmotte et al., "Global warming of 1.5°C," IPCC Special Report on climate change, desertification, land degradation, sustainable land management, food security, and greenhouse gas fluxes in terrestrial ecosystems, IPCC, Geneva, Switzerland, Oct. 2018.

[2] *Renewable Energy 3020*. Sejong, South Korea: Ministry Trade, Ind., Energy, Feb. 2017.

[3] L. G. Meegahapola, S. Bu, D. P. Wadduwage, C. Y. Chung, and X. Yu, "Review on oscillatory stability in power grids with renewable energy sources: Monitoring, analysis, and control using synchrophasor technology," *IEEE Trans. Ind. Electron.*, vol. 68, no. 1, pp. 519–531, Jan. 2021.

[4] S. Maihemuti, W. Wang, H. Wang, J. Wu, and X. Zhang, "Dynamic security and stability region under different renewable energy permeability in IENGS system," *IEEE Access*, vol. 9, pp. 19800–19817, 2021.

[5] B. Mahamedi, M. Eskandari, J. E. Fletcher, and J. Zhu, "Sequence-based control strategy with current limiting for the fault ride-through of inverter-interfaced distributed generators," *IEEE Trans. Sustain. Energy*, vol. 11, no. 1, pp. 165–174, Jan. 2020.

[6] Q. Salem, L. Liu, and J. Xie, "Dual operation mode of a transformerless H-bridge inverter in low-voltage microgrid," *IEEE Trans. Ind. Appl.*, vol. 55, no. 5, pp. 5289–5299, Sep./Oct. 2019.

[7] Z. Shuai, C. Shen, X. Yin, X. Liu, and Z. J. Shen, "Fault analysis of inverter-interfaced distributed generators with different control schemes," *IEEE Trans. Power Del.*, vol. 33, no. 3, pp. 1223–1235, Jun. 2018.

[8] Y. Geng, L. Zhu, X. Song, K. Wang, and X. Li, "A modified droop control for grid-connected inverters with improved stability in the fluctuation of grid frequency and voltage magnitude," *IEEE Access*, vol. 7, pp. 75658–75669, 2019.

[9] F. Cheng et al., "A comprehensive AC fault ride-through strategy for HVDC link with serial-connected LCC-VSC hybrid inverter," *CSEE J. Power Energy Syst.*, vol. 8, no. 1, pp. 175–187, Jan. 2022.

[10] M. I. Hossain and M. A. Abido, "Positive-negative sequence current controller for LVRT improvement of wind farms integrated MMC-HVDC network," *IEEE Access*, vol. 8, pp. 193314–193339, 2020.

[11] P. Cheng, K. Li, C. Wu, J. Ma, and L. Jia, "Flexible power regulation and limitation of voltage source inverters under unbalanced grid faults," *CES Trans. Elect. Mach. Syst.*, vol. 6, no. 2, pp. 153–161, Jun. 2022.

[12] A. Saleh, A. Rastegarnia, A. Farzamnia, and K. T. T. Kin, "Power and current limiting strategy based on droop controller with floating characteristic for grid-connected distributed generations," *IEEE Access*, vol. 10, pp. 13966–13973, 2022.

[13] T. Hathiyaldeniye, U. D. Annakkage, N. Pahalawaththa, and C. Karawita, "A comparison of inverter control modes for maintaining voltage stability during system contingencies," *IEEE Open Access J. Power Energy*, vol. 9, pp. 55–65, 2022.

[14] S. Lissandron, L. D. Santa, P. Mattavelli, and B. Wen, "Experimental validation for impedance-based small-signal stability analysis of single-phase interconnected power systems with grid-feeding inverters," *IEEE J. Emerg. Sel. Topics Power Electron.*, vol. 4, no. 1, pp. 103–115, Mar. 2016.

[15] S. Wang, Z. Liu, J. Liu, D. Boroyevich, and R. Burgos, "Small-signal modeling and stability prediction of parallel droop-controlled inverters based on terminal characteristics of individual inverters," *IEEE Trans. Power Electron.*, vol. 35, no. 1, pp. 1045–1063, Jan. 2020.

[16] A. Adib, B. Mirafzal, X. Wang, and F. Blaabjerg, "On stability of voltage source inverters in weak grids," *IEEE Access*, vol. 6, pp. 4427–4439, 2018.

[17] H. Alenius et al., "Hardware-in-the-loop methods for stability analysis of multiple parallel inverters in three-phase AC systems," *IEEE J. Emerg. Sel. Topics Power Electron.*, vol. 9, no. 6, pp. 7149–7158, Dec. 2021.

[18] X. Peng and H. Yang, "Stability analysis of multi-paralleled grid-connected inverters including distribution parameter characteristics of transmission lines," *CSEE J. Power Energy Syst.*, vol. 7, no. 1, pp. 93–104, Jan. 2021.

[19] B. Zhang, X. Du, J. Zhao, J. Zhou, and X. Zou, "Impedance modeling and stability analysis of a three-phase three-level NPC inverter connected to the grid," *CSEE J. Power Energy Syst.*, vol. 6, no. 2, pp. 270–278, Jun. 2020.

[20] K. D. Smith, S. Jafarpour, and F. Bullo, "Transient stability of droop-controlled inverter networks with operating constraints," *IEEE Trans. Autom. Control*, vol. 62, no. 2, pp. 633–645, Feb. 2022.

[21] X. Guo, Z. Lu, B. Wang, X. Sun, L. Wang, and J. M. Guerrero, "Dynamic phasors-based modeling and stability analysis of droop-controlled inverters for microgrid applications," *IEEE Trans. Smart Grid*, vol. 5, no. 6, pp. 2980–2987, Nov. 2014.

[22] W. Cao, Y. Ma, L. Yang, F. Wang, and L. M. Tolbert, "D–Q impedance based stability analysis and parameter design of three-phase inverter-based AC power systems," *IEEE Trans. Ind. Electron.*, vol. 64, no. 7, pp. 6017–6028, Jul. 2017.

[23] D. W. Hart, "Inverters," in *Power Electronics*, 1st ed. New York, NY, USA: McGraw-Hill, 2011, pp. 342–344.